NUMERICAL STUDY OF THUNDERSTORM ELECTRIFICATION WITH A THREE-DIMENSIONAL DYNAMICS AND ELECTRIFICATION COUPLED MODEL—MODEL DESCRIPTION AND PARAMETERIZATION OF ELECTRICAL PROCESSES*

SUN Anping (孙安平), *YAN Muhong* (言穆弘)**, *ZHANG Yijun* (张义军),

ZHANG Hongfa (张鸿发)

Cold and Arid Regions Environmental and Engineering Research Institute,

Chinese Academy of Sciences, Lanzhou 730000

and *HUANG Meiyuan* (黄美元)

Institute of Atmospheric Physics, Chinese Academy of Sciences, Beijing 100029

Received June 26, 2001

ABSTRACT

A new three-dimensional dynamics and electrification coupled model has been developed for investigating the characteristics of microphysics, dynamics and electrification inside thunderstorms. This model is basically modified from a three-dimensional, time-dependent, and dual-parameter cloud model originally established in IAP (Institute of Atmospheric Physics) and a two-dimensional axisymmetric cloud dynamics and electrification coupled model. Primary modifications to the model include not only the coupling of electrification with dynamical and microphysical processes, but also the lightning discharge process and screening layer effect at the cloud top as well. Apart from including a full treatment of small ions with attachment to six classes of hydrometeors, the inductive and non-inductive charging mechanisms are more specifically considered. A case simulation of July 19, 1981 CCOPE is performed aiming to validate the potential capability of the model. Comparison between model results and observations reveals that the model has the capacity to reproduce many of the observed characteristics of thunderstorms in dynamical, microphysical, and electrical aspects.

Key words: thunderstorm, electrification, parameterization, coupling

I. INTRODUCTION

During the past several decades, many efforts in the numerical modeling of electrification inside thunderstorms have been conducted since cloud models were originally

---

* Project supported by the National Natural Science Foundation of China (Grant No. 49975002), Cold and Arid Regions Environmental and Engineering Research Institute, Chinese Academy of Sciences (Grant No. 210037), and LSSR of Peking University.

** E-mail address: yanmh@ns.lzb.ac.cn

developed in the 1950s. Chiu (1978) and Orville and Kopp (1977) established a two-dimensional electrification and dynamics coupled model, in which warm and cold microphysical processes were considered. Takahashi (1984) incorporated ice microphysical processes and riming electrification mechanism in this model and discussed the electrification process occurring in a summer thunderstorm. The results showed that the polarity of the charge transfer in the collision was dependent on temperature and liquid water content. Below a critical temperature in the range -10 to -20°C, negative charge was transferred to graupel, while in warmer air positive charge was transferred. The updraft carries upward small ice particles forming the upper region of positive charge in thunderstorms. Helsdon and Farley (1987) investigated electrification processes in the thunderstorm occurring in Montana on July 19, 1981, and discussed the dependence of magnitude of charge transfer on microphysical and dynamical processes. Ziegler and MacGorman (1994) simulated the effectiveness of non-inductive charging mechanism in thunderstorms, and results showed that non-inductive charging mechanism was the important electrification process and dependent upon liquid water content. Yan et al. (1996a; 1996b) investigated the features of charge distribution and charging mechanisms inside the thunderstorm initiated with an ideal thermodynamic condition using a two-dimensional axisymmetric model and concluded that inductive, non-inductive, and secondary charging are three primary mechanisms to get the thunderstorm to become electrified. Schuur and Rutledge (2000) simulated the evolution of electrical structure in stratiform region in MCS (mesoscale convective system) occurring in Pre-Storm experiment, and pointed out that non-inductive ice-ice charge transfer in the low liquid water content region was sufficient to account for observed charge density magnitudes in MCS. As much as 70% of the total charge in the stratiform region was contributed by charge advection from the convective region.

However, the numerical researches mentioned above are all conducted using two-dimensional axisymmetic or slab-symmetric models. As many scientists showed before, only a symmetrically isolated single cell may be effectively simulated with axisymmetic models due primarily to without exchanges of energy and substance between cloud inside and outside. Meanwhile, the impact of heterogeneous surface on formation and development of thunderstorms can not be objectively examined with two-dimensional axisymmetric models. As such two-dimensional slab-symmetric models are more preferred to reveal the characteristics of convective systems strongly featured in two dimensions, such as squall lines etc., while the dynamics of actual thunderstorms is usually three-dimensional in nature. Wilhelmson (1972) compared the result of case study aiming to analyze the characteristics of convective development in mono-direction wind shear environment obtained from a three-dimensional cloud model with that from a two-dimensional slab-symmetric model, and pointed out that downdraft outside cloud may be significantly intensified and the whole life history of the storm was probably much shorter in two-dimensional simulations. In addition, several researches (e.g., Takahashi 1984) already showed that the separation of space charge in different polarity inside thunderstorms was closely related to development of cloud dynamics and microphysics which are normally not enough to be explained more clearly with two-dimensional cloud models. Even though Rawlins (1982) developed a three-dimensional, time-dependent electrification model associated with ice phase charging mechanisms, yet the relatively simplified parameterization of microphysics included in this model limited the interpretation of results.

In an effort to better understand the evolution of overall charge structure and possible charging mechanisms, and to discuss the features of hail growth inside electrically intensive thunderstorms, a new three-dimensional dynamics and electrification coupled model is first established on the basis of a three-dimensional cloud model and a two-dimensional axisymmetric cloud dynamics and electrification coupled model. Then a numerical simulation is undertaken to validate the model's capabilities with initial soundings taken from the Cooperative Convective Precipitation Experiment (CCOPE) on July 19, 1981. In this paper, model description, parameterizations of electrical processes, and preliminary comparison between observations and simulations are presented in detail in the following sections below. The detailed discussions concerning the evolution of electrical structure and the growth of hail particles in intensively electrical thunderstorms will be presented in follow-up paper.

II. MODEL DESCRIPTION

1. *Model Governing Equations*

Dynamical framework of the present model is similar to that established by Klemp and Wilhelmson (1978) except that three components of electrical force which are usually considered to be negligible in comparison with pressure gradient, frictional acceleration of precipitation particles, and initial buoyancy inside cumulonimbus, $E_x(\rho_T/\rho)$, $E_y(\rho_T/\rho)$ and $E_Z(\rho_T/\rho)$, are included in the momentum equations. That is, this model is a dynamics and electrification coupled model, which can be used to examine spatial and temporal characteristics of space charge in thunderstorms. The governing equations for momentum in the horizontal and vertical directions, thermodynamic energy, and mass continuity can be written as

$$\frac{\partial u_i}{\partial t} + u_j \frac{\partial u_i}{\partial x_j} = - C_p \bar{\theta}_v \frac{\partial \pi'}{\partial z} + \delta_{i3} g \left(\frac{\theta'_v}{\bar{\theta}_v} + 0.61 q'_v - q_t \right) + \frac{\rho_T}{\rho} E_i + D_{ui}, \tag{1}$$

$$\frac{\partial \theta}{\partial t} + u_j \frac{\partial \theta}{\partial x_j} = S_\theta + D_\theta, \tag{2}$$

$$\frac{\partial \pi'}{\partial t} + u_j \frac{\partial \theta}{\partial x_j} = - \frac{\bar{C}^2}{C_p \bar{\rho}\, \bar{\theta}_v^2} \frac{\partial \bar{\rho}\, \bar{\theta}_v u_j}{\partial x_j} - \frac{R_d}{C_v} \pi' \frac{\partial u_j}{\partial x_j} + \frac{C^2}{C_p \bar{\theta}_v^2} \frac{d\theta_v}{dt} + D_{\pi'}, \tag{3}$$

where u_i and E_i ($i = 1$, 2 and 3) represent the components of velocity and electric field strength in x, y and z directions, respectively, $\bar{\theta}_v$ is the basic-state virtual potential temperature, θ_v is the virtual potential temperature, q_t is the mixing ratio of total hydrometeors, q'_v is the perturbation water vapor, π' is the pressure perturbation, ρ is air density. S_θ represents the latent heat released as a result of water phase change. C, C_p, C_v, and R_d are adiabatic sound speed, specific heat of dry air at constant pressure and at constant volume, and gas constant for dry air, respectively. ρ_T is the total space charge density. The term D represents the subgrid turbulent mixing and the more detailed description can be found in Kong et al. (1990).

The prognostic equations for the mixing ratio of water vapor and the mixing ratio and number concentration of hydrometeors are written in the form of

$$\frac{\partial q_v}{\partial t} + u_j \frac{\partial q_v}{\partial x_j} = S_{q_v} + D_{q_v}, \tag{4}$$

$$\frac{\partial M_x}{\partial t} + u_j \frac{\partial M_x}{\partial x_j} = S_{M_x} + D_{M_x} + \frac{1}{\bar{\rho}} \frac{\partial}{\partial z}(\bar{\rho} M_x V_x), \tag{5}$$

where q_v is the mixing ratio of water vapor. M_x denotes the mixing ratio and number concentration of hydrometeors. V_x is the mass-weighted terminal velocities of hydrometeors. $\bar{\rho}$ is the basic-state air density as a function of z. Here x includes six hydrometeors cloud, rain, ice, snow, graupel and hail, respectively. S_{q_v} and S_{M_x} represent source and sink terms of microphysics for water vapor and different hydrometeors and are introduced specifically in Hong (1996; 1998).

The equations governing number concentration of ions are as follows:

$$\frac{\partial n_\pm}{\partial t} + u_j \frac{\partial n_\pm}{\partial x_j} = S_{n_\pm} + D_{n_\pm} \mp \frac{\partial (\mu_\pm E_x n_\pm)}{\partial x} \mp \frac{\partial (\mu_\pm E_y n_\pm)}{\partial y} \mp \frac{\partial (\mu_\pm E_z n_\pm)}{\partial z}, \tag{6}$$

where $n_\pm$ is the concentration of ions. $\mu_\pm$ is ion mobility depending on height. $S_{n_\pm}$ is the source and sink terms of ions. E_x, E_y and E_z are the components of electric field in x, y and z directions, respectively.

Each of six hydrometeors denoted by x in Eq. (5) is allowed to have a charge associated with it. The governing equation for charge density of each hydrometeor is

$$\frac{\partial q_{xe}}{\partial t} + u_j \frac{\partial q_{xe}}{\partial x_j} = S_{q_{xe}} + D_{q_{xe}} + \frac{1}{\bar{\rho}} \frac{\partial}{\partial z}(\bar{\rho} V_x q_{xe}), \tag{7}$$

where q_{xe} denotes the charge density carried by each hydrometeor. $S_{q_{xe}}$ is the source and sink of charge density, and $D_{q_{xe}}$ is the subgrid turbulent mixing of charge density.

Then the electric field can be obtained by following equations:

$$\rho_T = e(n_+ - n_-) + \sum q_{xe}, \tag{8}$$

$$\frac{\partial^2 \varphi}{\partial x^2} + \frac{\partial^2 \varphi}{\partial y^2} + \frac{\partial^2 \varphi}{\partial z^2} = \frac{\rho_T}{\varepsilon}, \tag{9}$$

$$E_x = -\frac{\partial \varphi}{\partial x}, \quad E_y = -\frac{\partial \varphi}{\partial y}, \quad E_z = -\frac{\partial \varphi}{\partial z}, \tag{10}$$

where φ is the electric potential, and ε is the scalar electrical permittvity of air.

2. *The Source and Sink Terms of Charge Density of Ions and Each HydroMeteor*

$$S_{n_\pm} = G - \alpha n_+ n_- - \left(\frac{\partial n_\pm}{\partial t}\right)_e^c - \left(\frac{\partial n_\pm}{\partial t}\right)_e^i - \left(\frac{\partial n_\pm}{\partial t}\right)_e^r - \left(\frac{\partial n_\pm}{\partial t}\right)_e^h - \left(\frac{\partial n_\pm}{\partial t}\right)_e^g - \left(\frac{\partial n_\pm}{\partial t}\right)_e^s, \tag{11}$$

$$S_{q_{ce}} = e\left[\left(\frac{\partial n_+}{\partial t}\right)_c^e - \left(\frac{\partial n_-}{\partial t}\right)_c^e\right] - \left(\frac{\partial q_{re}}{\partial t}\right)_p^{r-c} - \left(\frac{\partial q_{he}}{\partial t}\right)_{np}^{h-c} - \left(\frac{\partial q_{ge}}{\partial t}\right)_{np}^{g-c} - \left(\frac{\partial q_{se}}{\partial t}\right)_p^{s-c}, \tag{12}$$

$$S_{q_{ie}} = e\left[\left(\frac{\partial n_+}{\partial t}\right)_e^i - \left(\frac{\partial n_-}{\partial t}\right)_e^i\right] - \left(\frac{\partial q_{he}}{\partial t}\right)_p^{h-i} - \left(\frac{\partial q_{ge}}{\partial t}\right)_p^{g-i} - \left(\frac{\partial q_{he}}{\partial t}\right)_{np}^{h-i} - \left(\frac{\partial q_{ge}}{\partial t}\right)_{np}^{g-i} +$$

$$\left(\frac{\partial q_{he}}{\partial t}\right)_s^{h-i} + \left(\frac{\partial q_{ge}}{\partial t}\right)_s^{g-i} - \left(\frac{\partial q_{se}}{\partial t}\right)_p^{s-i}, \tag{13}$$

$$S_{q_{re}} = e\left[\left(\frac{\partial n_+}{\partial t}\right)_e^r - \left(\frac{\partial n_-}{\partial t}\right)_e^r\right] + \left(\frac{\partial q_{re}}{\partial t}\right)_p^{r-c}, \tag{14}$$

$$S_{q_{se}} = e\left[\left(\frac{\partial n_+}{\partial t}\right)_e^s - \left(\frac{\partial n_-}{\partial t}\right)_e^s\right] - \left(\frac{\partial q_{se}}{\partial t}\right)_p^{s-c} + \left(\frac{\partial q_{se}}{\partial t}\right)_p^{s-i} - \left(\frac{\partial q_{se}}{\partial t}\right)_{np}^{g-s} - \left(\frac{\partial q_{se}}{\partial t}\right)_{np}^{h-s}, \tag{15}$$

$$S_{q_{ge}} = e\left[\left(\frac{\partial n_+}{\partial t}\right)_e^g - \left(\frac{\partial n_-}{\partial t}\right)_e^g\right] + \left(\frac{\partial q_{ge}}{\partial t}\right)_p^{g-i} + \left(\frac{\partial q_{ge}}{\partial t}\right)_{np}^{g-i} + \left(\frac{\partial q_{ge}}{\partial t}\right)_{np}^{g-s} + \left(\frac{\partial q_{ge}}{\partial t}\right)_{np}^{g-c} + \left(\frac{\partial q_{ge}}{\partial t}\right)_s^{g-c}, \tag{16}$$

$$S_{q_{he}} = e\left[\left(\frac{\partial n_+}{\partial t}\right)_e^h - \left(\frac{\partial n_-}{\partial t}\right)_e^h\right] + \left(\frac{\partial q_{he}}{\partial t}\right)_p^{h-i} + \left(\frac{\partial q_{he}}{\partial t}\right)_{np}^{h-i} + \left(\frac{\partial q_{he}}{\partial t}\right)_s^{h-c} + \left(\frac{\partial q_{he}}{\partial t}\right)_{np}^{h-c} + \left(\frac{\partial q_{he}}{\partial t}\right)_{np}^{h-s}, \tag{17}$$

where $\left(\frac{\partial n_\pm}{\partial t}\right)_e^x$, $\left(\frac{\partial q_{xe}}{\partial t}\right)_p^{x-y}$, $\left(\frac{\partial q_{xe}}{\partial t}\right)_{np}^{x-y}$, and $\left(\frac{\partial q_{ie}}{\partial t}\right)_s$ represent ion diffusion and ion selective capture, inductive, non-inductive and secondary ice electrification, respectively. The superscripts x in $\left(\frac{\partial n_\pm}{\partial t}\right)_e^x$ include all six kinds of hydrometeors, and x and y in $\left(\frac{\partial q_{xe}}{\partial t}\right)_p^{x-y}$ and $\left(\frac{\partial q_{xe}}{\partial t}\right)_{np}^{x-y}$, represent the two types of water substances between which charge is transferred.

III. PARAMETERIZATIONS OF ELECTRICAL PROCESSES

1. *Electrification Processes*

(1) *Ion diffusion and selective capture mechanisms*

Due to cosmic ray and surface radioactivity generation, there exist a great number of positive and negative ions suspending in atmosphere. The hydrometeors can be charged in different polarity by attaching positive or negative ions driven by heat diffusion. In addition, as being polarized in preexisting electric field, hydrometeors are featured to carry different polarity charges on their upper and lower surfaces. Because of differences in terminal velocities of hydrometeors and in ion mobility, ions are optionally attracted to be attached to hydrometeors. Normally these two charging processes are considered simultaneously in electrification models. The variation in number concentration of ions due to these two charging processes can be written as

$$\left(\frac{\partial n_\pm}{\partial t}\right)_e^x = \overline{N}_x\left[\left(\frac{\partial n_\pm}{\partial t}\right)_D^x + \left(\frac{\partial n_\pm}{\partial t}\right)_{EC}^x\right], \tag{18}$$

where superscript x represents hydrometeors including cloud, rain, ice, snow, graupel, and hail, respectively. Subscripts D and EC denote ion diffusion and ion selective capture mechanisms. $\overline{N}_x$ is the averaged number concentration of hydrometeors.

Based on the idea from Gunn (1954), the number concentration of ion attached to all kinds of hydrometeors due to ion diffusion mechanism can be described in the form:

$$\left(\frac{\partial n_\pm}{\partial t}\right)_D^x = \pm \frac{4\pi q_x \mu_\pm n_\pm}{\exp(\pm q_x e / r_x kT) - 1}. \tag{19}$$

When $|q_x| << \frac{r_x KT}{e}$, Eq. (19) can be changed to

$$\left(\frac{\partial n_\pm}{\partial t}\right)_D^x = 4\pi r_x D_\pm n_\pm N_x \left[1 + \left(\frac{r_x V_x}{2\pi D_\pm}\right)^{0.5}\right], \tag{20}$$

where r_x, V_x, and N_x represent the radius, terminal velocity and number concentration of hydrometeors, respectively. $D_\pm$ and $\mu_\pm$ are heat diffusion coefficients and small ion mobility for positive and negative ions.

According to the idea of Chiu (1978), the number concentration of ion attached to hydrometeors due to selective ion capture charging mechanism can be formulated as follows in terms of different direction of vertical electric field and magnitude of charge density of hydrometeors.

1) When $\overline{q_{xe}} > q_{xe} > -\overline{q_{xe}}$ and the direction of vertical electric field is the same as that of terminal velocity of hydrometeors, we have

$$\left(\frac{\partial n_-}{\partial t}\right)_{EC}^x = 3\pi n \mu_- |E_z| r_x^2 \left[1 + \frac{q_{xe}}{\overline{q_{xe}}}\right]^2, \tag{21}$$

$$\left(\frac{\partial n_+}{\partial t}\right)_{EC}^x = \begin{cases} 3\pi n_+ \mu_+ |E_z| r_x^2 \left[1 - \frac{q_{xe}}{\overline{q_{xe}}}\right]^2, & |V_x| < \mu_+ |E_z| \\ \frac{-n_+ \mu_+ q_{xe}}{\varepsilon}, & q_{xe} \leqslant 0, \quad |V_x| > \mu_+ |E_z| \\ 0. & q_{xe} > 0, \quad |V_x| > \mu_+ |E_z| \end{cases} \tag{22}$$

2) When $\overline{q_{xe}} > q_{xe} > -\overline{q_{xe}}$ and the direction of vertical electric field is opposite to that of terminal velocity of hydrometeors, we have

$$\left(\frac{\partial n_+}{\partial t}\right)_{EC}^x = 3\pi n_+ |E_z| r_x^2 \left[1 - \frac{q_{xe}}{\overline{q_{xe}}}\right]^2, \tag{23}$$

$$\left(\frac{\partial n_-}{\partial t}\right)_{EC}^x = \begin{cases} 3\pi n_- \mu_- |E_z| r_x^2 \left[1 + \frac{q_{xe}}{\overline{q_{xe}}}\right]^2, & |V_x| < \mu_- |E_z| \\ \frac{n_- \mu_- q_{xe}}{\varepsilon}, & q_{xe} > 0, \quad |V_x| > \mu_- |E_z| \\ 0. & q_{xe} \leqslant 0, \quad |V_x| > \mu_- |E_z| \end{cases} \tag{24}$$

3) When $q_{xe} > \overline{q_{xe}}$ the variations of number concentration of positive and negative ions are the following

$$\left(\frac{\partial n_-}{\partial t}\right)_{EC}^x = \frac{n_- \mu_- q_{xe}}{\varepsilon}, \tag{25}$$

$$\left(\frac{\partial n_-}{\partial t}\right)_{EC}^x = 0. \tag{26}$$

4) When $q_{xe} < \overline{q_{xe}}$ the variations of number concentration of positive and negative ions are the following

$$\left(\frac{\partial n_+}{\partial t}\right)_{EC}^x = -\frac{n_+ \mu_+ q_{xe}}{\varepsilon}, \tag{27}$$

$$\left(\frac{\partial n_-}{\partial t}\right)^x_{EC} = 0. \tag{28}$$

where $\overline{q_{xe}} = 12\pi\varepsilon r_x^2 |E_z|$. ε is the electrical permittivity of air. Subscript EC denotes ion selective capture mechanism. Superscript x includes cloud, rain, ice, snow, graupel, and hail, respectively.

(2) *Inductive charging mechanism*

In the presence of a pre-existing electric field inside thunderstorms, cloud and precipitation particles become charged in different polarity in lower and upper surfaces. When a smaller particle collides with a larger one and rebounds, the charge transfer between two particles occurs and the magnitude and sign of transferred charge are totally dependent upon the ambient electric field strength and its orientation with respect to the particles.

Assuming a smaller particle with radius r_S collides with a larger particle with radius r_L, the transferred charge between them is written as

$$\Delta q = 4\pi\varepsilon\Gamma_1 |\boldsymbol{E}| \cos(\boldsymbol{E}, \boldsymbol{r}_{LS}) r_S^2 + Aq_{Le} - Bq_{Se}, \tag{29}$$

$$A = \frac{\Gamma_2\left(r_S/r_L\right)^2}{1+\Gamma_2\left(r_S/r_L\right)^2}, \tag{30}$$

$$B = \frac{1}{1+\Gamma_2\left(r_S/r_L\right)^2}, \tag{31}$$

where $\Gamma_1 = \pi^2/2$ and $\Gamma_2 = \pi^2/6$. $\boldsymbol{r}_{LS}$ is the vector along the line joining the centers of the two particles at the time of impact. q_L (q_S) is the charge already existing on the larger (smaller) particle.

A single larger hydrometeor may interact with many smaller particles, so the integrated charge for larger particle per unit time over the volume swept out by the larger particle can be described as

$$\frac{\delta q_{Le}}{\delta t} = -\int E_f |\boldsymbol{V}_{LS}| N_S \Delta q S(\alpha_1) \mathrm{d}A, \tag{32}$$

where E_f is the collision efficiency between the two particles, $|\boldsymbol{V}_{LS}|$ is the relative impact speed, N_S is the number concentration of the smaller particles. $S_{\alpha 1}$ is the angle-dependent separation probability. $\mathrm{d}A$ is collision interactive section and can be formulated as

$$\mathrm{d}A = r_L^2 \sin\alpha_1 \cos\alpha_2 \mathrm{d}\alpha_1 \mathrm{d}\alpha_2, \tag{33}$$

and there is the following expression in spherical coordinate system

$$\cos(\boldsymbol{E}, r_{LS}) = \sin\alpha_1 \sin\alpha_2 \sin(\boldsymbol{E}, \boldsymbol{V}_{LS}) - \cos\alpha_1 \cos(\boldsymbol{E}, \boldsymbol{V}_{LS}). \tag{34}$$

Substitution Eqs. (25), (29) and (30) into Eq. (28), then Eq. (28) can be written as

$$\frac{\delta q_{Le}}{\delta t} = E_f |\boldsymbol{V}_{LS}| N_S (2\pi r_L^2) \int_{\alpha=0}^{\pi/2} \sin\alpha_1 \cos\alpha_1 \{4\pi\varepsilon_0 \Gamma_1 |\boldsymbol{E}| \cos(\boldsymbol{E}, \boldsymbol{V}_{LS})\ r_S^2 \cos\alpha_1 - Aq_{Le} + Bq_{Se}\} S(\alpha_1) \mathrm{d}\alpha_1. \tag{35}$$

Defining $\langle S \rangle$ as the average separation probability and $\langle \cos\alpha \rangle$ as the average value of $\cos\alpha$:

$$\langle S\rangle = \int_0^{\pi/2} S(\alpha_1)2\pi r r_L^2 \sin\alpha_1 \cos\alpha_1 d\alpha_1/\pi r_L^2, \tag{36}$$

$$\langle \cos\alpha_1\rangle = \int_0^{\pi/2} 2S(\alpha_1)\sin\alpha_1\cos^2\alpha_1 d\alpha_1/\langle S\rangle. \tag{37}$$

Substitution Eqs. (32) and Eq. (33) into Eq. (31) and carrying out the integration of Eq. (31) result in the following expression for the charge accumulated by a precipitation hydrometeor

$$\left(\frac{\partial q_{Le}}{\partial t}\right)_p^{L-S} = E_{LS}|V_L - V_S|N_S N_L \pi r_S^2 \cdot [4\varepsilon\Gamma|\boldsymbol{E}|\cos(\boldsymbol{E},\boldsymbol{V}_{LS})r_S^2\langle\cos\alpha\rangle - Aq_{Le} + Bq_{Se}]\langle S\rangle, \tag{38}$$

where V_L and V_S are terminal velocity of the larger and smaller particle. Subscript p denotes inductive mechanism. Superscript $L-S$ represents two kinds of hydrometeors colliding with each other, and includes hail-ice, graupel-ice, hail-cloud, graupel-cloud, rain-cloud, snow-ice, and snow-cloud, respectively. In current version of this model, the average separation probability $\langle S\rangle$ is still temporarily assumed a constant or temperature-dependent variable as shown in Table 1.

Table 1. Parameters Associated with Inductive and Non-Inductive Charging Mechanisms

Interaction	Non-inductive A' (C)	Inductive $\langle S\rangle$ (Separation probability)
	Dry growth mode	
Graupel and hail/ cloud (riming)	$\begin{cases} -2\times10^{15} & T_c>-10°C \\ 2\times10^{15} & T_c<-10°C \end{cases}$	0.9
Graupel and hail/ snow	$\begin{cases} -2\times10^{13} & T_c>-10°C \\ 2\times10^{13} & T_c<-10°C \end{cases}$	$1-\exp(0.09T_c)$
Graupel and hail/ice	$\begin{cases} -2\times10^{14} & T_c>-10°C \\ 2\times10^{14} & T_c<-10°C \end{cases}$	0.9
	Wet growth mode	
Graupel and hail/cloud (shedding)	0.0	$\left(\frac{\text{Amount Shed}}{\text{Amount Accreted}}\right)$
Graupel and hail/rain (all shed or limited accretion)	0.0	$\begin{cases} 1.0 & \text{if all shed} \\ 1.0-\left(\frac{\text{Amount Frozen}}{\text{Amount Accreted}}\right) & \text{if limited accretion} \end{cases}$

(3) *Non-inductive charging mechanism*

So far many numerical investigations (e.g. Takahashi 1978; Kuettner et al. 1982) associated with thunderstorm electrification were particularly focused on non-inductive changing mechanism in that a great number of laboratory and field experiments have exhibited that accumulated charge transferred resulting from non-inductive charging mechanism accounts considerably for the total space charge in thunderstorms. In addition, more importantly, it is also shown in laboratory studies that the magnitude and sign of charge transferred are generally determined by so-called reverse-temperature, liquid water content and impact speed. In this model, the experiment result of Takahashi (1978) for reverse-temperature has been applied specifically.

Same as that in inductive charging mechanism, the charge transferred due to non-inductive mechanism between a smaller and a larger particle is

$$\Delta q = - A' + (B - 1)q_{Le} - Bq_{Se}. \tag{39}$$

All terms in Eq. (39) have same meaning as before except for A' which is constant and shown in Table 1. With aids of Eqs. (33), (34) and (39), as such (32) can be changed into

$$\left(\frac{\partial q_{Le}}{\partial t}\right)_{np}^{L-S} = E_{LS}|V_L - V_S|N_L N_S \pi r_L^2 (S)[A' + (B - 1)q_{Le} + Bq_{Se}], \tag{40}$$

where subscript np represents non-inductive mechanism. Superscript $L-S$ represents two kinds of hydrometeors colliding with each other, and includes hail-ice, graupel-ice, hail-cloud, graupel-cloud, graupel-snow, and hail-snow, respectively.

(4) *Secondary ice charging mechanism*

On the basis of experiment results aiming to examine the role of secondary ice-particle production during riming as well as rime-particle collision with ice crystals on rime deposit charging, Hallett (1979) concluded that the average magnitude of charge transferred is approximately 10^{-14} C. As such, the polarity of transferred charge is largely related to environment temperature and liquid water content. In accordance with Hallett (1979), the charge transferred is written as

$$\left(\frac{\partial q_{Le}}{\partial t}\right)_{s}^{L-i} = 3\rho F_c \delta q / 4\pi r_i^3 \rho_w, \tag{41}$$

where F_c is content of secondary ice, δq is charge transferred during each collision between larger particles and secondary ice particles. ρ and ρ_w represent densities of air and water. Subscript s denotes secondary ice charging mechanism, and superscript $L-i$ represents ice particles colliding with another larger hydrometeor L. Currently hail and graupel are considered to be involved in this mechanism.

2. *Discharge Processes*

Discharge parameterization is required for storm electrification simulations beyond initial electrification. Without lightning discharges, the electric field can reach unrealistic magnitudes. A number of lightning parameterizations have been developed previously and here in this model the idea of Helsdon et al. (1992) has been adopted to handle this unrealistic magnitudes problem. This parameterization makes a single, unbranched channel which traces the electric field line from an initiation point. In accordance with observational results, the minimum electric field for initiating lightning discharge is set to 300 kV m^{-1}. The channel is extended until the ambient field falls below a certain threshold 150 kV m^{-1}. Then a relatively complicated analytical expression below is used to calculate the positive and negative linear charge densities that are induced by the external electric field along the channel.

$$Q'_n = -\left\{2\pi\varepsilon\frac{b^2}{a}\left[\frac{F'_1(a)P_1(x) - F'_3(a)P_3(x)}{f_1(a)p_1(x) - f_3(a)p_3(x)}\right]\right\}(\Phi - \Phi_0), \tag{42}$$

where Q'_n and Φ are the linear charge density and electrical potential at the grid involved in discharge channel. Φ_0 is the electrical potential at the initiation point. a and b represent the radius and half of length of lightning channel, respectively. $P_1(x)$ and $P_3(x)$ are Legendre functions of the first kind and x denotes the ratio between the length from initiation to grid point considered and whole length of channel. Four terms $f_1(a)$, $f_2(a)$, $F'_1(a)$, and $F'_3(a)$ are respectively formulated as follows:

$$\begin{aligned} f_1(a) &= \frac{5R^2a}{3} - \frac{3a^2}{5}, & f_2(a) &= \frac{2a^3}{3}, \\ F'_1(a) &= f'_1(a) - \frac{f_1(a)}{Q_1(y)}Q'_1(y), & F'_3(a) &= f'_3(a) - \frac{f_3(a)}{Q_3(y)}Q'_3(y), \end{aligned} \tag{43}$$

where R is the radius of equivalent spheroid. $Q_1(y)$ and $Q_3(y)$ are the Legendre function of the second kind. y is defined as $y=a/(a^2-b^2)^{1/2}$.

The charge at the ends of channel is first adjusted to maintain net charge neutrality of the flash, then converted to volume charge density by integration as follows

$$Q_T = Q_n\Delta l = Q'_n\int_0^{\Delta l}\int_{-2\Delta y}^{2\Delta y}\int_{-2\Delta x}^{2\Delta x} e^{-lx^2}\mathrm{d}x\mathrm{d}y\mathrm{d}z, \tag{44}$$

where Q_T is the charge density at each grid point included in lightning discharge channel.

3. *Parameterization of Screening Effect at Cloud Top*

Due to the presence of thunderstorms in which conductivity is a little bit different from that in fair environment, there exists a discontinuity in electric conductivity inside and outside the cloud top. To neutralize this discontinuity, normally negative ions outside thunderstorms are preferentially attracted toward cloud top and accumulated eventually leading to forming a negative screen layer. Based on charge density continuity equation, the variation of charge density for a screen charge layer with thickness L can be formulated as

$$\frac{\partial\rho}{\partial t} = -\frac{J_c - J_a}{L} = -\frac{\sigma_c E_c - \sigma_a E_a}{L}, \tag{45}$$

where σ_c and σ_a are electric conductivities inside thunderstorms and fair weather, respectively. E_c and E_a are the vertical electric field strength inside and outside thunderstorms. With the aids of Gaussian law, the following two expressions can be used to adjust the vertical electric field strength at the grid near cloud top resulting from screen charge layer effect.

$$\begin{aligned} E_a^t &= E_a^{t-1} - \delta\zeta/2\varepsilon \approx E_a^{t-1} - L\delta\rho/2\varepsilon, \\ E_c^t &= E_c^{t-1} + \delta\zeta/2\varepsilon \approx E_c^{t-1} + L\delta\rho/2\varepsilon, \end{aligned} \tag{46}$$

where superscripts t and $t-1$ represent current and previous integration time step. $\delta\rho$ is determined by the following

$$\delta\rho = \frac{(2\varepsilon/L)\delta J^{t-1}}{\sigma_a + \sigma_c}\{1 - \exp[-(\sigma_a + \sigma_c)\Delta t/2\varepsilon]\}. \tag{47}$$

4. *Modification of Terminal Velocity of Hydrometeors*

In addition to being subject to downward gravitational force and upward frictional resistance, the larger precipitation particles are also forced by the vertical component of electrical force in electrically intensive thunderstorms. The expression of terminal velocities is formulated as

$$v_x = \left(\frac{8\pi r_x^2 g(\rho_i - \rho_a)}{3\pi r_x^2 C_D \rho_a} + \frac{2q_{xe}E_z}{\pi r_x^2 C_D \rho_a} \right)^{\frac{1}{2}}. \tag{48}$$

As for cloud drops and ice particles whose terminal velocities are usually considered to be negligible in normal cumulus model, the terminal fall speeds are balanced by the vertical electric force and frictional resistance in the form:

$$v_y = \frac{q_{ye}E_z}{6\pi\rho r_y \gamma}. \tag{49}$$

In Eqs. (48) and (49) subscript x includes rain, graupel and hail, and y consists of cloud and ice. C_D is drag coefficient. ρ, ρ_a, and ρ_i are densities of liquid water, the air, and ice particles, respectively. $q_{x(y)e}$ represents the charge density of hydrometeors. $r_{x(y)}$ is the radius of hydrometeors.

IV. INITIAL AND BOUNDARY CONDITIONS

In this model the standard staggered mesh by Klemp and Wilhelmson (1978) was adapted in which thermodynamic, moisture and electrical variables are defined at a common point and the velocity components are displaced by one-half grid interval. In solving the compressible equations of motion, time splitting method is used. For the horizontal and vertical advection terms, fourth-order and second-order finite differences are used. For Eq. (9), super relaxation method is used to determine electric potential as follows:

$$\varphi_{i,j,k}^{t+1} = (1 - \bar{\omega})\varphi_{i,j,k}^{t} + \frac{\bar{\omega}}{4 + 2\frac{L^2}{h^2}} \times$$

$$\left[\varphi_{i+1,j,k} + \varphi_{i-1,j,k} + \varphi_{i,j+1,k} + \varphi_{i,j-1,k} + \frac{L^2}{h^2}(\varphi_{i,j,k+1} + \varphi_{i,j,k-1})\right] + \frac{\rho_T L^2}{\varepsilon}, \tag{50}$$

where $\bar{\omega}$ is relaxation coefficient. L and h are grid spacing for horizontal and vertical dimensions, respectively. $\varphi_{i,j,k}^{t}$ is electric potential at given grid point, and subscripts i, j, and k represent the coordinate of grid point, while superscript t denotes integration time step.

The model domain is 17.5 km×17.5 km×18.5 km with a horizontal grid size of 1000 m and a vertical grid size of 500 m. The large and small time steps are 10 s and 2 s, respectively. The boundary conditions relevant to dynamics are detailedly described in Kong et al. (1990) and not presented here.

1. *Initial Conditions*

It is assumed that an initial steady state exists with ion production due to cosmic ray generation, ion loss due to recombination, and ion transport due to conduction in the ambient electric field all balancing. Then the vertical ion concentration can be derived as

$$n_{\pm}^{0} = \frac{-1.7 \times 10^{7}}{E_z^{00}(\mu_{+} + \mu_{-})} + \frac{10^{4} E_z^{00} \mu_{+}}{9.6\pi(\mu_{+} + \mu_{-})}, \tag{51}$$

where $E_z^{00} = -150$ V m^{-1}. The initial vertical distribution of electric field is assumed fair-weather profile as follows

$$E^{0} = E_z^{00} \exp(-2 \times 10^{-4} z). \tag{52}$$

2. *Boundary Conditions*

At the lateral boundaries, we assumed that the normal mixing term and horizontal electric field are equal to zero. At the lower boundary, consistent with the assumption that the earth's surface is a flat conducting plane, the potential is set to zero. At the model top, all variables except for vertical component of electric field and the ion concentration are assumed to be zero, while the vertical component of electric field and the ion concentration are maintained undisturbed at their initial values. The potential at the top of the model is obtained by integrating the following expression over the depth of the domain and employing Eq. (52) for the electric field profile:

$$\Psi = -\int_{0}^{Z_{\mathrm{top}}} E^{0} \mathrm{d}z. \tag{53}$$

V. VALIDATION OF PRELIMINARY RESULTS

The basic-state wind, temperature and moisture profiles used in the numerical simulation are taken from observations in Montana on July 19, 1981 during Cooperative Convective Precipitation Experiment (CCOPE) project (Fig. 1). Using this sounding is beneficial because detailed observational analyses of this case have been represented by several studies (e. g., Jones et al. 1982; Gardiner et al. 1985; Dye et al. 1986) and simulated results can be directly compared with observations. Convection is initiated using a warm bubble in the lowest 2 km of the model with a maximum magnitude of 1.5°C. Numerical integration is carried out for 90 min.

As shown in Fig. 1, a relatively weakly unstable layer with maximum magnitude of temperature 1.5°C is present between 625 hPa and 425 hPa. Therefore, this thermodynamic environment is favorable to developing a locally short-lived thunderstorm. Figure 2 is the vertical cross-section of total water content and space charge density through the center of the cloud in y-direction at $t=30$ min and $t=42$ min. The simulation time is shown in the upper left corner of each figure. The results indicate that the cloud originally forms at $t=21$ min (cloud water content larger than 0.1 g m^{-3}) with higher temperature approximately 20°C at cloud base. At $t=24$ min, rain starts to appear at a height of 3.0 km through autoconversion from cloud to rain. The cloud develops vertically up to 6.0 km and the maximum total water content area is located at a height of 4.5 km with the maximum magnitude of 6.0 g m^{-3} at $t=30$ min (Fig. 2a). At this time, the cloud is exclusively composed of liquid water substances because it is totally located in the area with temperature higher than 0°C. With updraft more intensified, the cloud top reaches its maximum height of 12.4 km and the maximum total water content area becomes more

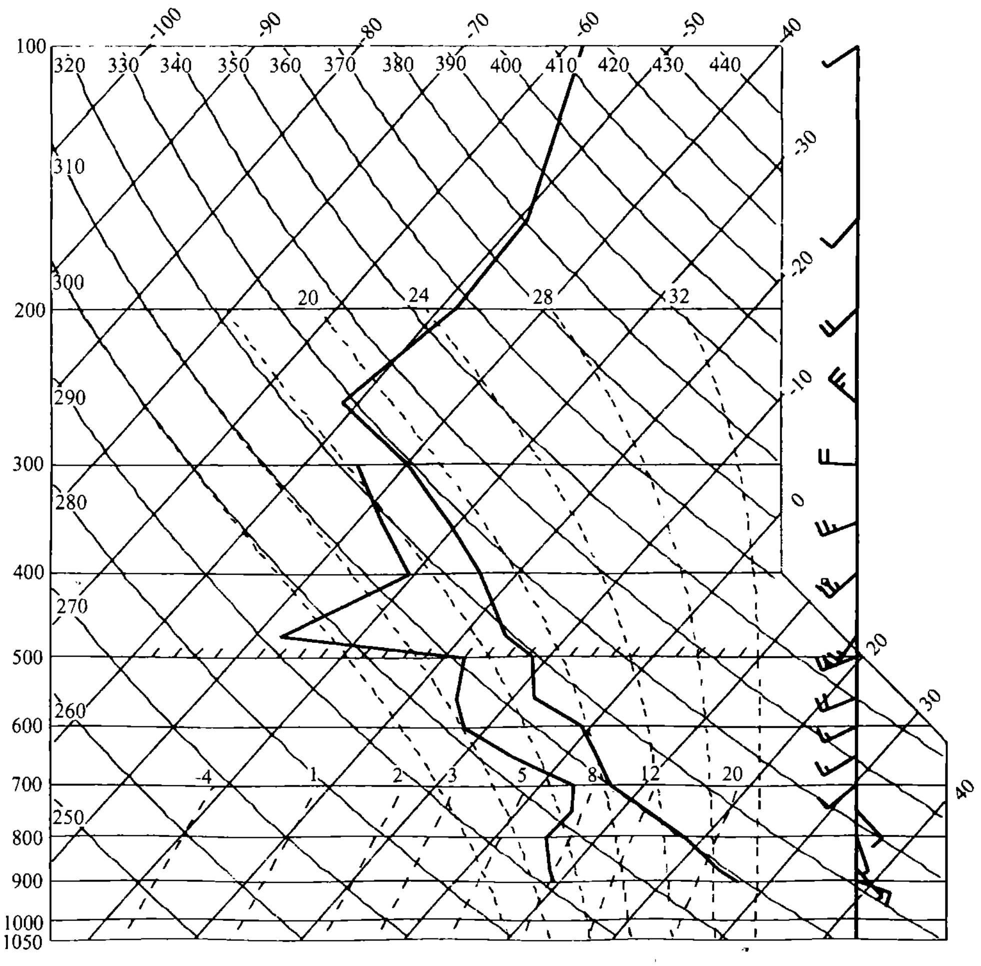

Fig. 1. The skew T-log P diagram of the basic-state thermodynamic sounding.

extensive in vertical direction, from 4.0 km to 8.0 km, with the maximum magnitude of 10.0 g m^{-3} at $t=42$ min. In addition, the cloud is distinguishingly characterized by cloud anvil (Fig. 2b). The initial negative charge center appears at a height of 3.0 km with the maximum value of 0.023 nC m^{-3} at $t=30$ min (Fig. 2c). The resulting vertical electric field at $t=30$ min provides a much stronger environment for the inductive charging mechanism. At $t=42$ min, the triple polarity electrical structure, in which the main negative charge zone at about 6.2 km is located between 12.0 km uppel-level and 4.5 km lower-level regions of positive charge, is obviously already established (Fig. 2d). The maximum magnitude of positive charge density and the minimum magnitude of negative charge density are 0.4 nC m^{-3} and -1.35 nC m^{-3}, respectively. Dye et al. (1986) pointed out that the cloud top reached a height of approximate 10.2 km and the maximum negative charge area was located at 5.8 km half an hour later after this cloud initially formed. It is shown clearly that the observed is basically qualitatively consistent with the fact appearing in the actual cloud. Figure 3 is time series of domain maximum magnitude of total electric field. It is exhibited that electric field strength increases relatively slower due primarily to

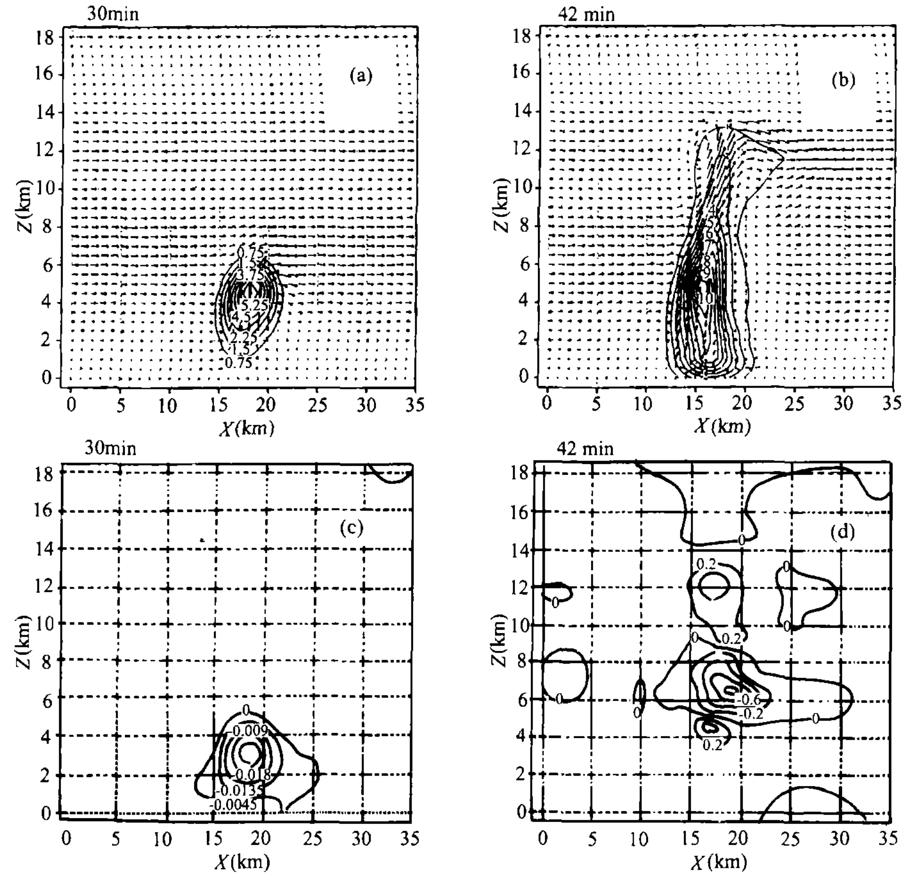

Fig. 2. The vertical cross-section of total water content and space charge density through the center of the cloud in y-direction at $t=30$ min and $t=42$ min.

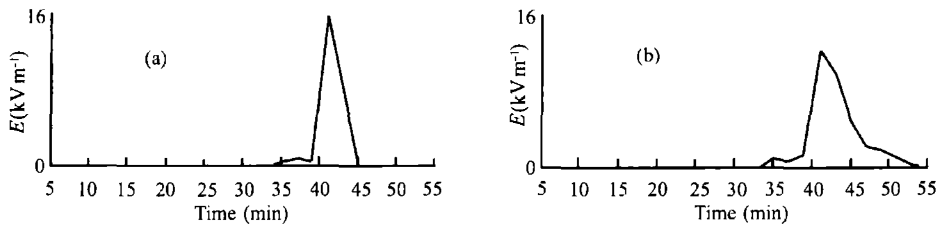

Fig. 3. Time series of domain maximum magnitude of total electric field. (a) observation; (b) simulation.

weaker electrification process prior to 39 min. However, it starts to increase dramatically after 40 min because there exist a variety of ice-phase particles that are beneficial to intensify charging rate inside the cloud. At $t = 42$ min, the total electric field reaches its maximum in whole life history with the observed value of 16 kV m^{-1} and simulated value of 13 kV m^{-1}. Although the simulated total electric field is somewhat smaller than the observed, both of them have good agreement in the trend of variation. Much of the microphysical, dynamical and electrical characteristics of the cloud detected by aircraft measurement are generally reproduced in the numerical simulation. Therefore, it is possible to study dynamical, microphysical and electrical processes of thunderstorms with this model and the results are basically credible.

REFERENCES

Chiu, C. S. (1978). Numerical study of cloud electrification in an axisymmetric time-dependent cloud model. *J. Geophys. Res.*, **83**: 5025—5049.

Dye, J. E., Jones, J. J., Winn, W. P., Cerni, T. A., Gardiner, B., Lamb, D., Pitter, R. L., Hallett, J. and Saunders, C. P. R. (1986), Early electrification and precipitation development in a small, isolated Montana cumulonimbus, *J. Geophys. Res.*, **91**: 1231—1247.

Gardiner, B., Lamd, D., Pitter, R. L. and Hallett, J. (1985), Measurements of initial potential gradient and particle charges in a Montana summer thunderstorm, *J. Geophys. Res.*, **90**: 6079—6086.

Gunn, R. (1954). Diffusion charging of atmospheric droplets by inos and the resulting combination coefficinets, *J. Meteor.*, **11**: 339.

Hallett, J. and Saunders (1979), Charge separation associated with secondary ice crystal production, *J. Atmos. Sci.*, **38**: 2470—2484.

Hallett, J. (1979). Charge seperation associated with secondary ice crystal production, *J. Atmoss. Sci.*, **36**: 2230—2235.

Helsdon, J. H., Jr. and Farley, R. D. (1987), A numerical modeling study of a Montana thunderstorm: 2. Model results versus observations involving electrical aspects, *J. Geophys. Res.*, **92**: 5661—5675.

Helsdon, J. H., Wu, G. and Farley, R. D. (1992), An intracloud lightning parameterization scheme for a strom electrification model. *J. Geophys. Res.*, **97**: 5865—5884.

Hong Yanchao (1996), Numerical study of strato-cumulus mixing cloud, (I) Model and parameterization of microphysical processes, *Acta Meteor. Sinica*, **54**: 544—557 (in Chinese).

Hong Yanchao (1998), A three dimensional catalysis hail cloud model, *Acta Meteor. Sinica*, **56**: 641—650 (in Chinese).

Jones, J. J., Winn, W. P. and Dye, J. E. (1982), Early electrification in a cumulus, Proceeding of 9th Conference on Cloud Physics, American Meteorological Society, Boston, 562pp.

Klemp, J. B. and Wilhelmson, R. B. (1978), The simulation of three-dimensional convective storm dynamics, *J. Atmos. Sci.*, **35**: 1070—1096.

Kong Fangou, Huang Meiyuan and Xu Huaying (1990), A three dimensional study of ice-phase processes in a convective cloud, *Chinese J. Atmos. Sci.*, **14**: 441—453 (in Chinese).

Kuettner, J. R., Zev Levin and Sartor, J. D. (1982), Thunderstorm electrification—inductive or non-inductive, *J. Atmos. Sci.*, **38**: 2470—2484.

Orville, H. D. and Kopp, F. J. (1977), Numerical simulation of the life history of a hailstorm, *J. Atmos. Sci.*, **34**: 1596—1618.

Rawlins, F. (1982), A numerical study of thunderstorm electrification using a three-dimensional model incorporating the ice phase, *Quant. J. Roy. Meteor. Soc.*, **108**: 779—800.

Schuur, T. J. and Rutledge, S. A. (2000), Electrification of stratiform regions in mesoscale convective systems. Part II: Two-dimensional numerical model simulations of a symmetric MCS, *J. Atmos. Sci.*, **57**: 1983—2006.

Takahashi, T. (1984): Thunderstorm electrification—A numerical study, *J. Atmos. Sci.*, **41**: 2541—2558.

Takahashi, T. (1978), Riming electrification as a charge generation mechantsm in thunderstorms, *J. Atmos. Sci.*, **35**, 1536—1548.

Wilhelmoson, R. (1972), The numerical simulation of a thunderstorm cell in two-and three-dimensions. Ph. D. Thesis, University of Illinois.

Yan Muhong, Guo Changming and Ge Zhengmo (1996a). Numerical study of cloud dynamic-electrification in an axisymmetric, time-dependent cloud model, I. Theory and model. *Chinese J. Geophys. Res.*, **39**: 52—64 (in Chinese).

Yan Muhong, Guo Changming and Ge Zhengmo (1996b). Numerical study of cloud dynamic-electrification in an axisymmetric, time-dependent cloud model, II. Results and Analysis. *Chinese J. Geophys. Res.*, **39**: 65—78 (in Chinese).

Ziegler, C. L. and MacGorman, D. R. (1994). Observed lightning morphology relative to modeled space charge and electric field distributions in a tornadic storm. *J. Atmos. Sci.*, **51**: 833—851.